Western United States Water Resources

Detecting Springs in Nevada, California, and Colorado for Detection and Research using NASA Earth observations

Spring 2025 | Colorado – Fort Collins
April 4th, 2025

Authors: Greta Bolinger, Colin Murphy, Pallavi Pokharel, Geena Poulter

Abstract: Spring ecosystems are crucial in arid regions, providing freshwater, supporting biodiversity, and maintaining hydrological cycles. However, monitoring these ecosystems proves difficult due to their remote locations and the costly nature of conducting labor-intensive field surveys. This project investigated the feasibility of using NASA Earth observations to detect and monitor spring ecosystems in the Mojave National Preserve (California), Black Rock Desert National Conservation Area (Nevada), and the San Juan Mountains (Colorado). In collaboration with the United States Geological Survey, Bureau of Land Management, National Park Service, and The Two Frontiers Project, this study aimed to improve decision-making in conservation, land use, and spring monitoring. Using Landsat and 3DEP satellite data, the team analyzed indices such as the Normalized Difference Vegetation Index (NDVI) and, Normalized Difference Moisture Index (NDMI), land surface temperature (LST), and included topography indices to identify springs. The team applied detection and suitability models, including Random Forest, Maximum Entropy, and Generalized Linear Models, and cross-referenced them with known spring locations. The results showed that known springs correlated with lower drainage density, higher NDVI, higher NDMI, cooler temperatures, higher elevations, and shallower slopes. While satellite imagery showed promise for spring monitoring, the feasibility remained limited by spatial resolution constraints, field data quality, seasonal variability, and classification errors. Overall, the study demonstrated the potential of combining remote sensing and field data to support conservation and management of spring ecosystems.

Key Terms: Landsat, hydrology, remote sensing, detection model, springs detection, seasonality, MaxEnt, GLM, RandomForest

Advisors: Dr. Anthony Vorster (Colorado State University, Natural Resource Ecology Laboratory), Dr. James Henriksen (The Two Frontiers Project), Dr. Paul Evangelista (Colorado State University, Natural Resource Ecology Laboratory), Dr. Catherine Jarnevich (USGS, Fort Collins Science Center), Nicholas Young (Colorado State University, Natural Resource Ecology Laboratory), Christopher Tsz Hin Choi (Colorado State University, Natural Resource Ecology Laboratory)

Lead: Truman Anarella (Colorado – Fort Collins)

1. Introduction

1.1 Background Information & Project Partners

Spring ecosystems are seasonal, emergent hydrological features that support ecosystem biodiversity in the American West. Springs are physically small, appearing as subtle features on satellite imagery. Many springs remain unmapped and unmonitored, creating uncertainty regarding future water availability and habitat health (Dhakal et al., 2024). Frequent surveying of springs and surrounding ecosystems is essential for resource management and policy-making decisions made by government agencies.

Due to their small size and ephemeral nature, spring ecosystems can be challenging to distinguish from the surrounding landscape. Certain environmental factors, like vegetative health, elevation, the degree of slope and aspect, land surface temperature, and drainage density have been shown to help predict the distribution of spring ecosystems (Niraula et al., 2020; Reath & Ramsey, 2013; Dhakal et al., 2024). Many of these environmental factors can be derived from satellite imagery through remote sensing. Remote sensing is a powerful tool that can be used for hydrological monitoring of springs as it allows for large-scale detection of anomalies thought to be associated with springs (Williams & Jackson, 2007). Studies have used remote sensing of thermal imagery to identify temperature anomalies associated with thermal springs (Idi et al., 2022). Surface reflectance satellite imagery has been analyzed, with success, to show anomalies in normalized difference vegetation index (NDVI) and normalized difference moisture index (NDMI), both of which could provide insight into seasonally stable areas of vegetation that may be associated with spring ecosystems (Castell Azzi et al., 2024). Alongside field-based observations of known spring locations, remote sensing of key environmental factors affecting spring distribution may offer a unique opportunity to detect spring ecosystems throughout the American West.

This project partnered with the United States Geological Survey (USGS) Colorado Water Science Center, the Bureau of Land Management (BLM) Winnemucca District Office, the National Park Service (NPS) Mojave National Preserve, and The Two Frontiers Project (2FP), a Colorado-based research nonprofit exploring microbial diversity in extreme environments. Each project partner conducted ground-based surveys of spring ecosystems within their respective geographic boundaries. The partners were interested in detecting and monitoring spring ecosystems for natural resource management. NPS and BLM prioritized wildlife conservation and community water resource management, while 2FP sought to identify springs that exhibited extreme characteristics, such as unique algal coloration or gaseous emission.

Due to challenges with routine sampling of remote backcountry spring ecosystems, project partners were interested in using remote sensing and machine learning tools to detect, classify, and predict the distribution of spring ecosystems throughout the American West. Machine learning models, such as Random Forest, Generalized Linear Model (GLM), and Maximum Entropy (MaxEnt), have all been shown to enhance ecosystem-based suitability detection (Granata et al., 2018), and offer an improved method of mapping suitable spring locations. Project partners were interested in utilizing an integrated remote sensing and machine learning model approach to inform the location of future field surveys for long-term monitoring of springs.

1.2 Study Area & Period

The team detected seasonal changes in spring ecosystems over a single year (2024) across three study areas. The team had originally planned to analyze springs from 2000-2024, as project partners aimed to gain an enhanced understanding of how climate change impacted springs within their geographic boundaries (Zhuang et al., 2024). Due to a lack of consistent field data availability from project partners across those years, however, project partners agreed to narrow the study period to the year 2024 and examine seasonal changes to spring ecosystems.

The study areas for this project included: the Mojave National Preserve, the Black Rock Desert, and the San Juan Mountain region, reflecting the jurisdiction areas of the project partners (Figure 1). The Mojave National Preserve, located in southeastern California, is a point of convergence for the Mojave, Great Basin, and

Sonoran deserts, and is managed by the National Park Service. This region is well known for its geologic history, including volcanic fields and sand dunes, while its topography covers dry riverbeds and mountain ranges (U.S. National Park Service, n.d.). The Black Rock Desert is a National Conservation Area managed by the Bureau of Land Management in northwestern Nevada; it is known for its 200 square miles of desert backcountry, which was once the bed of Lake Lahontan (Black Rock Desert-High Rock Canyon Emigrant Trails National Conservation Area, n.d.). The San Juan Mountain region in southwest Colorado is known for its high desert mesas as well as its alpine peaks and volcanic activity that created many of the calderas that are now seen today (USFS, n.d.; Lipman et al., 1973). The United States Geological Survey collects, researches, and distributes information the hydrological resources of the San Juan Mountains.

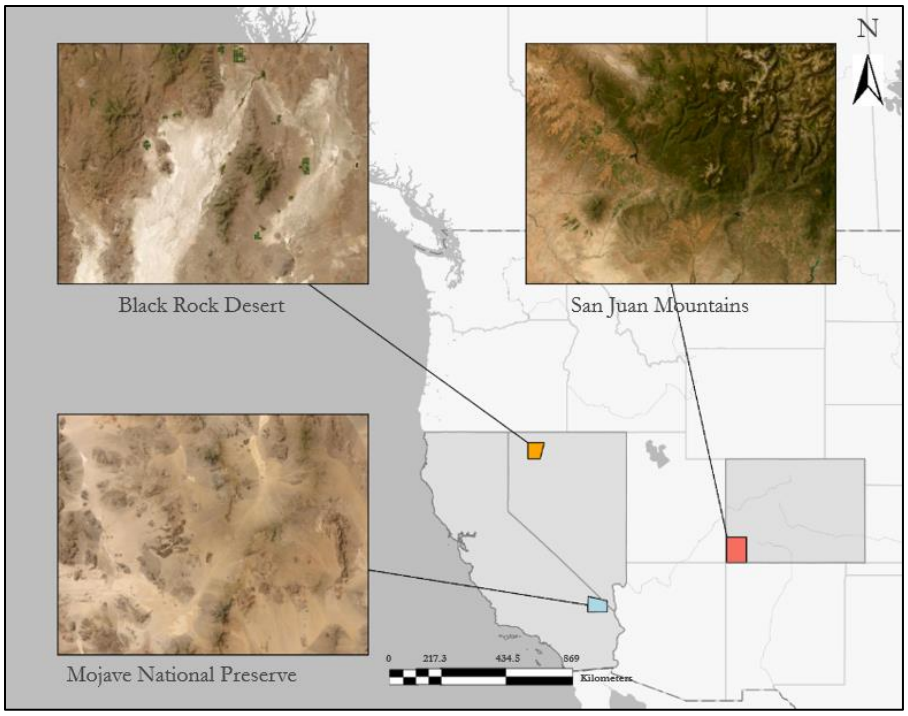

Figure 1. *Map of the entire study area, including the Mojave, Black Rock, and San Juan sites. The imagery was derived from ArcGIS Pro 2.1.0. Basemap credits: Esri, USGS, sources: Earthstar Geographics, Esri, TomTom, Garmin, FAO, NOAA, USGS, EPA, and USFWS.*

1.3 Feasibility & Project Objectives

The primary goal of this project was to assess the feasibility of monitoring springs in the Western United States using remote sensing. The first objective was to identify NASA Earth observations, remote sensing tools, and geospatial datasets that may be useful in mapping spring ecosystems. The second objective was to use an integrated remote-sensing and machine learning approach to create a predictive map showing suitable spring locations throughout the Western United States.

2. Methodology

2.1 Data Acquisition

The team chose to focus on several predictor variables to aid in the suitability mapping of spring distribution. To quantify the topographic influence on spring distribution, the team chose to acquire elevation data, which was used to calculate slope, aspect, and drainage density. The team chose to acquire, process, and analyze surface reflectance and thermal band data to investigate vegetation changes and thermal emissivity associated with known spring locations. Specifically, the team chose to acquire thermal data for its use in calculating land surface temperature (LST), as springs may exhibit distinct thermal signatures compared to their surrounding environment. In arid environments, cooler signatures could indicate groundwater influence, while in colder

seasons, warmer spots may suggest spring activity. When combined with NDVI, LST may aid in differentiating between spring-fed vegetation and seasonal vegetation, as spring-fed vegetation remains green longer than seasonal vegetation.

2.1.1 NASA Earth observations

The team sourced satellite data from dates representing the wet and dry seasons of 2024(Table 1). In the Mojave Desert, the wet season (e.g., Dec 15, 2024) aligned with winter rainfall from Pacific storms, while summer was dry (e.g., Sep 26, 2024) (U.S. National Park Service, n.d.). In the Black Rock Desert, the wet season (e.g., Mar 14, 2024) occurred in late winter, due to accumulated snowmelt, and the dry season (e.g., Sep 30, 2024) occurred after peak summer heat (USGS, n.d.). For the San Juan Mountains, the wet season (e.g., Mar 22, 2024) aligned with peak snowpack and early melt, while the dry season (e.g., Sep 14, 2024) followed the end of the summer monsoons and temperatures (San Juan Mountains Association, n.d.; Weather Spark, n.d.; USFS, n.d.).

The team acquired NASA Earth Observation surface reflectance and thermal data from Operational Land Imager (OLI) and Thermal Infrared Sensors (TIRS) aboard Landsat 8 and 9 satellites. Specifically, the team accessed and downloaded surface reflectance data. This was obtained from the Landsat 8-9 OLI/TIRS Collection 2 Level 2 Surface Reflectance 30m raster 2024 available through USGS EarthExplorer (U.S. Geological Survey, 2024) and included bands 4, 5, and 6 from the OLI sensor and band 10 from TIRS. When downloading, the team selected images that had the smallest percentage of cloud cover relative to mapped area, with the search ranging from 0%-10%.

The team used 3D Elevation Program Shuttle Radar Topography Mission (SRTM), Level 2 10m Digital Elevation Model TIF, 2024. The team accessed and downloaded this data across all three study sites, using The National Map Downloader, courtesy of USGS (USGS National Map Downloader, 2024).

Table 1. NASA Earth observations for the San Juan Mountains (SJ), Black Rock Desert (BR) and Mojave National Preserve (MOJ)

Data Type	Variables	Sensor/ Platform	Product Level	Spatial Resolution	Winter (Wet) 2024 Date	Summer (Dry) 2024 Date	Data Source
Surface Reflectance	NDVI, NDMI	Landsat 8/9 OLI	Level 2	30m	**SJ:** 3/22	**SJ:** 9/14	USGS Earth Explorer
					BR: 3/14	**BR:** 9/30	
					MOJ: 12/15	**MOJ:** 9/26	
Thermal	LST	Landsat 8/9 TIRS	Level 2	30m	**SJ:** 3/22	**SJ:** 9/14	USGS Earth Explorer
					BR: 3/14	**BR:** 9/30	
					MOJ: 12/15	**MOJ:** 9/26	
DEM (NED)	Elevation, Slope, Aspect, Drainage Density	3DEP (varied sources)	Level 2	10m	n/a	n/a	USGS National Map Downloader

2.1.2 Ancillary Data

The team also used ancillary datasets, including a geo-referenced, spring location points layer contributed by each project partner. All spring location datasets contained geographic coordinates of each spring, as well as unique attributes, such as the year that the project partners collected the data, or the name of the spring. Mojave National Preserve included the results of a near decade-long (2007-2015) "wet hand test" in their spring locations dataset, indicating the spring water level, or, more specifically, whether one could fully submerge their hand (1) or not (0) in each of their spring locations. Black Rock Desert BLM included the elevation of each spring, while the Two Frontiers Project included quantitative measures of unique minerals and algal assemblages associated with each spring.

To represent seasonal moisture conditions across the study areas, the team incorporated evapotranspiration data from the Standardized Precipitation and Evapotranspiration Index (SPEI). To derive SPEI values for the study sites, the team first accessed the evapotranspiration dataset from the Climate Engine website and downloaded the relevant Gridded Surface Meteorological (GridMET) data in raster format. The team then used ArcGIS Pro, version 3.2.0 to geospatially generate the evapotranspiration layers. The team then used the Clip Raster tool in ArcGIS Pro to clip the raster layers to the three study sites. After clipping, the evapotranspiration raster was exported as .tif files.

2.2 Data Processing

The team used a suite of geoprocessing software and tools to process NASA Earth observations and other satellite imagery. Specifically, the team used geoprocessing toolboxes in ArcGIS Pro, containing tools like "Raster Calculator," "Clip," (Figure 2), and "Reproject," which were supplemented by Open-Access software like QGIS, version 3.40.0 – Bratislava (equipped with the GDAL package) and R to process and visualize our data (QGIS Development Team, 2018).

To prepare our data for analysis, the team applied specific methods to each dataset to generate our predictor variables: elevation, slope, aspect, NDVI, NDMI, LST, and drainage density. The team initially considered the SPEI dataset but ultimately filtered it out of the Black Rock Desert and San Juan Mountain models due to redundancy with other moisture-related indices. Using the "r.slope.aspect" tool within the QGIS GRASS package, the team calculated the slope by comparing each pixel elevation to eight surrounding pixels. Slopes were expressed in degrees (º). 0º slopes indicated flat land, while slopes of 70º or more indicated steep, cliff-like terrain. Aspect data were calculated in terms of "Northness" (-1 (south-facing) to +1 (north-facing)) and "Eastness" (-1 (west-facing) to +1 (east-facing)) (Table 2).

Table 2
Environmental parameter processing to produce spring predictor variables

Index	Formula
NDVI	$\frac{(NIR + Red)}{(NIR - Red)}$
NDVI Seasonal Difference	$NDVI_{wet} - NDVI_{dry}$
NDMI	$\frac{(NIR + SWIR)}{(NIR - SWIR)}$
NDMI Seasonal Difference	$NDVI_{wet} - NDVI_{dry}$
LST	$(Band10 * 0.00341802) + 149.0) - 273.15) \times 1.8 + 32)$
Aspect Northness	$\cos(aspect * \pi/180)$
Aspect Eastness	$sin(aspect * \pi/180)$
Drainage Density Stream Extraction	$FlowAcc > 1000$

The team calculated NDVI using the Near-Infrared (Band 5) and Red (Band 4) bands, while NDMI was derived from the Near-Infrared (Band 5) and Shortwave Infrared (Band 6) bands. To geospatially generate NDVI and NDMI layers within ArcGIS Pro, version 3.2.0, the team used the Raster Calculator tool (Esri, 2024) to calculate NDVI and NDMI. For NDVI and NDMI, the team generated raster layers for both the wet and dry seasons, subtracting the dry season raster from the wet to show the seasonal change in each (Table 2). Negative NDVI difference values indicated healthier vegetation in the dry season than in the wet season, allowing the team to zero in on these locations to attempt to identify springs that may have been responsible for this dry season greening. Similarly, the team chose to calculate NDMI differences to reveal where more positive NDMI difference values indicated higher surface moisture and potential spring locations, while also highlighting water resource-limited regions (Table 2). The team also calculated Drainage Density to evaluate subsurface water movement and groundwater discharge potential, revealing regions with potentially high flow accumulation, as well as regions with active drainage, both of which helped determine potential spring locations (Table 2).

The team also used Raster Calculator to calculate LST from the Thermal Band 10. This process involved multiplying the values of the raster by the rescaling factor of 0.00341802 and adding 149.0 to convert the values into degrees Kelvin (Table 2). To convert LST from degrees Kelvin to degrees Fahrenheit, the LST value was subtracted from 273.15 to convert to degrees Celsius and then multiplied by 1.8 and added to 32.0.

To derive Drainage Density from the Digital Elevation Model, the team first used the Fill tool (Esri, 2024) to remove depressions in the DEM. The team then used the Flow Direction tool (Esri, 2024) to indicate the direction of water flow, followed by employing the Flow Accumulation (Esri, 2024) tool to calculate upstream flow contribution. The streams were then extracted using the Raster Calculator to identify areas with high flow accumulation, which identified areas with sufficient flow accumulation to be considered a "stream channel" (Table 2). Next, the team used the Raster to Polyline tool (Esri, 2024) to convert "stream channels" into vector format, followed by the Line Density tool (Esri, 2024) to create the final raster by calculating the concentration of streams per unit area.

The team also created a geo-referenced layer of 10,000 pseudo-absence spring points representing locations in which springs are not likely to be detected, based on the characteristics of each known spring location (Figure 2). To do so, the team used the Kernel Density tool in the Spatial Analyst toolbox in ArcGIS Pro (Esri, 2024) to generate a raster layer showing a density heat map derived from our field data points. The kernel density layer was manipulated by the Multi-Dimensional Scaling (MDS) Builder in SAHM, which specified the generation of 10,000 background points representing pseudo-absence springs that trained the model on where not to predict spring locations.

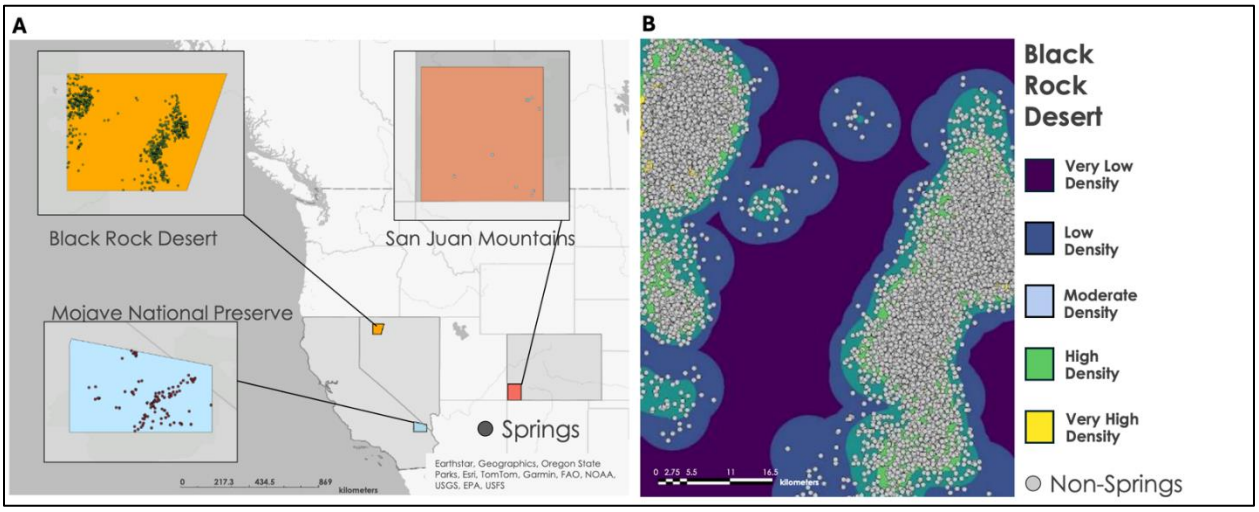

Figure 2. *Map of all* ***A.*** *known spring locations across the entire study area and* ***B.*** *non-spring locations, or pseudo-absence*

points, in the Black Rock Desert. The imagery was derived from ArcGIS Pro 2.1.0. Basemap credits: Esri, USGS, Sources: Earthstar Geographics, Esri, TomTom, Garmin, FAO, NOAA, USGS, EPA, and USFWS.

2.3 Data Analysis

Due to the physically vast regions covered by our three study sites and spring suitability detection needs of our project partners, the team tested a diverse array of analyses to discover which would be most feasible for project partners. Specifically, the team analyzed the geospatial data using a combination of descriptive statistics and detection models.

First, the team generated histograms and boxplots to visualize the distribution of field data relative to the non-spring, model-generated, pseudo-absence points. These boxplots also served to visualize the relationship between known spring locations and each predictor variable. Further, the team calculated descriptive statistics (mean and standard error) for each predictor variable and compared the known spring values to the non-spring values using a t-test, indicating which predictor variables might drive the model output, based on their statistically significant ($p<0.05$) difference between the model's presence and absence training data.

Finally, the team applied three predictive suitability and detection models, Random Forest (RF), Maximum Entropy (MaxEnt), and Generalized Linear Model (GLM), to describe the distribution of springs across study sites. To do so, the team used a Java-based package called Software for Assisted Habitat Modeling (SAHM), which is available as an extension of VisTrails (open-source modeling software) and documented by Colin and Marian Talbert of USGS, Fort Collins Science Center (2001). The SAHM assisted in analyzing each predictor variable's significance, relative to other predictor variables, in formulating a prediction of spring locations throughout the study area and period (Morissette et al., 2013). SAHM reported these correlations as R^2 values, which corresponded to the final weighting of each predictor variable in generating a predictive map of spring locations. For each area of interest, the results of each model were added together to create an ensemble map depicting model agreement. A Multivariate Environmental Similarity Surface (MESS) was used to generate unreliable data zones where models were less accurate, which was overlaid on each ensemble map.

3. Results

3.1 Analysis of Results

The team first analyzed the value of each satellite-derived spring predictor variable geospatially associated with the existing spring distribution. The goal of these preliminary analyses was to understand the environmental parameters characterizing each spring ecosystem, for example the average land surface temperature associated with springs in the Black Rock Desert (Figure A1). Next, the team modeled suitable spring locations across the three study sites. The goal of each model (Random Forest, GLM, and MaxEnt) was to predict suitable locations for partner spring monitoring surveys, based on patterns in environmental characteristics commonly associated with spring ecosystems.

3.1.1 Spring Predictor Variables Determine Surrounding Environmental Characteristics

Analysis of the NDVI difference around known spring locations across the three study sites revealed distinct patterns in vegetation health. In the San Juan Mountains, NDVI showed a more negative seasonal difference, indicating a greater decline in vegetation health between the wet and the dry seasons (Figure A2A). In contrast, both the Black Rock Desert and the Mojave National Preserve showed NDVI differences closer to 0.0, suggesting that the vegetation in these regions remains relatively stable throughout the year. For NDMI, Black Rock Desert exhibited the highest difference, suggesting a larger increase in moisture at spring locations compared to the surrounding area (Figure A2B). On the other hand, the San Juan Mountains showed a negative NDMI difference, indicating lower moisture at spring sites. The Mojave National Preserve showed a slight positive NDMI difference, suggesting a modest increase in moisture levels.

Similarly, the team analyzed the Land Surface Temperature data, revealing temperature variations across the study areas, with LST values indicating a range of temperatures, including some cooler areas (Figure A3). The

analysis revealed similar temperature patterns across all three sites, where LST differences are influenced by topography; higher elevations tend to have cooler temperatures than lower-lying valleys. The data showed that springs are generally located around cooler areas.

The team analyzed known spring locations in relation to elevation data and observed that springs in the three study sites are distributed across a range of elevations but tend to cluster within specific elevation bands (Figure A4A). Springs are predominantly found at mid to high elevations in all three sites. The analysis showed that most known springs are located on shallower slopes (Figure A4B). The Black Rock Desert showed the highest variability in slope, while the San Juan Mountains showed the lowest. Known spring locations across all three sites also indicated that springs are usually found on aspects with a slight south and west-facing aspect, just below zero (Figure A4C). At all three sites, the springs correlated with areas of low drainage density rather than high. In each location, the known spring locations suggest that the springs are found in regions where the drainage density is lower. This pattern is true across all three areas, where low drainage density does not allow water to flow away as rapidly.

3.1.2 Model Performance Statistics

Although all models generated spring suitability predictions, model accuracy varied across study sites (Table 3) with metrics derived from confusion matrices (Figure B1). In terms of accuracy, among the three models, the Random Forest model was best for accuracy (i.e., agreement with reference data) for Mojave National Preserve and Black Rock Desert based on Kappa scores of 0.15 and 0.23 respectively. On the other hand, none of the models demonstrated strong accuracy for the San Juan region.

Table 3

Comparison of the best-performing models for spring detection across Mojave National Preserve, Black Rock Desert, and the San Juan Mountains.

Study Area	Model	Percent Correctly Classified	AUC	Sensitivity	Specificity	Kappa
Mojave National Preserve	MaxEnt	76.37	0.83	0.73	0.76	0.05
	Random Forest	94.29	0.82	0.42	0.95	0.15
	GLM	76.48	0.71	0.60	0.77	0.04
Black Rock Desert	MaxEnt	68.62	0.74	0.67	0.69	0.18
	Random Forest	87.26	0.76	0.26	0.94	0.23
	GLM	64.51	0.70	0.64	0.65	0.13
San Juan Mountains	MaxEnt	67.05	0.69	0.61	0.67	0.02
	Random Forest	96.13	0.56	0	0.97	-0.01
	GLM	66.69	0.63	0.33	0.67	0.001

Overall, the MaxEnt model consistently performed better and was the most consistent in finding new data from the train split as compared to other models (Table 3). In the Mojave National Preserve, the maxent had a higher AUC score (0.83), demonstrating a higher capacity in distinguishing springs from pseudo-absence springs. In addition, its high sensitivity score (0.73) demonstrated that the model effectively detected spring presence. In the Black Rock Desert, MaxEnt achieved a slightly higher sensitivity of 0.672, with GLM at 0.64, while Random Forest showed a significantly lower sensitivity of 0.26. In the San Juan Mountains, MaxEnt again led with a sensitivity of 0.612, higher than both Random Forest (0.56) and GLM (0.33), further

confirming its relative success in accurately detecting spring locations across different study areas. Across all three sites, MaxEnt consistently showed high and stable values for AUC, sensitivity, and specificity for both the training run and the cross validation run, making it the most suitable model for detecting true positives (Figure B4).

The ensemble maps that were created further highlight areas of agreement between models, showing regions with the highest likelihood of spring presence and emphasizing the spatial consistency of predictions (Figure 3). NDVI and topographic variables played key roles in predicting spring presence, with NDVI emerging as one of the strongest predictors (Figure B2). The overall predictive capabilities of all three models were limited in the San Juan Mountains. This limitation was indicated by low AUC and Kappa values, which demonstrated weak ability to distinguish between spring and non-spring locations; a result of model overfitting (Figure 3C).

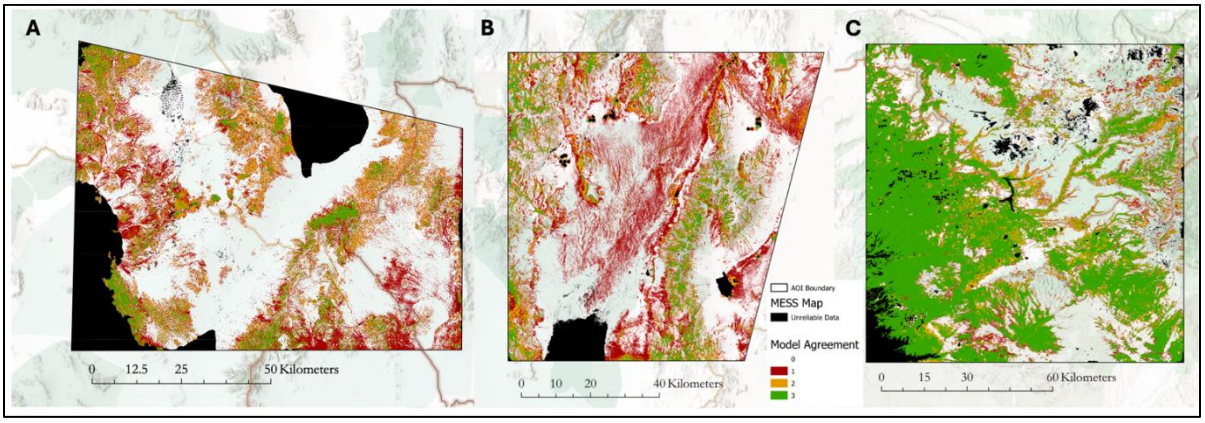

Figure 3. Ensemble map depicting habitat suitability model agreement on springs: (1) One Model Agrees on Presence, (2) Two Models Agree on Presence, (3) All Models Agree on Presence. **A.** Mojave National Preserve, **B.** Black Rock Desert, and **C.** the San Juan Mountain Region. Basemap credits: Esri, CGIAR, USGS, Sources: Esri, TomTom, Garmin, FAO, NOAA, USGS, © OpenStreetMap contributors, and the GIS User Community, California State Parks, Esri, TomTom, Garmin, SafeGraph, FAO, METI/NASA, USGS, Bureau of Land Management, EPA, NPS, USFWS.

The overall predictive capabilities of all three models were limited in the San Juan Mountains. This limitation was indicated by low AUC and Kappa values, which demonstrated the model's weak ability to distinguish between spring and non-spring locations. The latter, as shown as a high percentage of green (Figure 3C), or model agreement, was most likely a result of model overfitting due to the lack of presence training points.

3.2 Errors & Uncertainties

One of the most notable limitations in our project was the spatial resolution of Landsat data. For our study needs (large study area, multiple sites, multiple bands, etc.), 30-meter resolution was one of the best open-source options available. This, however, made analysis on a smaller scale challenging. Detecting anomalies such as small springs within individual pixel groups as a spectral or thermal signature in a desert ecosystem was not feasible with 30-meter resolution (Figure 4).

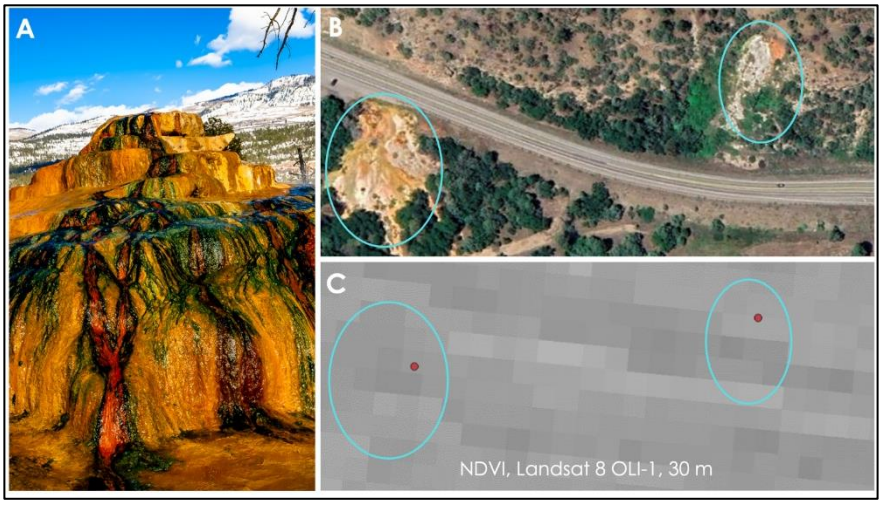

Figure 4. Case study of 30 m satellite imagery spatial resolution limitations to detect anomalies in spring predictor variables. **A.** Pinkerton Springs, a mineral and geothermal spring in Durango, Colorado. **B.** Scarring to the otherwise vegetated landscape, caused by Pinkerton Springs. **C.** Spring-induced scarring is not reflected as an anomaly on the vegetative health index at 30 m spatial resolution of Landsat 8&9 OLI 1&2 satellite imagery.

Because this project was a feasibility study, the team further investigated the Pinkerton Springs case study to see whether the vegetative scarring appeared as an NDVI anomaly on higher-resolution, 10-meter Sentinel 2 satellite imagery. Due to the large size of Pinkerton Springs, the 10-meter Sentinel 2 satellite imagery captured the spring-induced vegetative scarring as an anomaly, showing promise for high-resolution detection of larger springs (Figure 5). In comparison, with Landsat imagery, however, the small scene size and lack of thermal data captured by sensors aboard the Sentinel 2 satellite reduced its relevance to this project, which covered large study areas and required thermal bands.

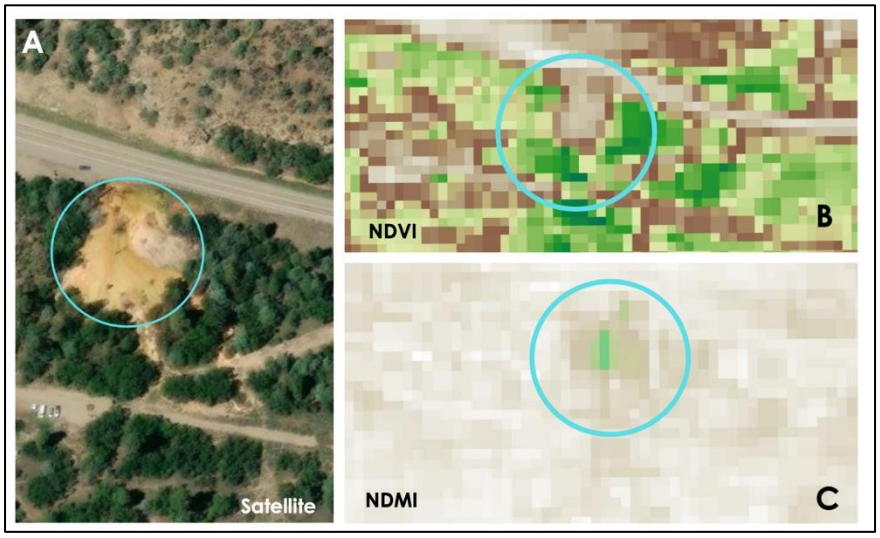

Figure 5. Case study of 10 m satellite imagery spatial resolution limitations to detect anomalies in spring predictor variables. **A.** Pinkerton Springs, a mineral and geothermal spring in Durango, Colorado. **B.** Scarring to the otherwise vegetated landscape, caused by Pinkerton Springs. **C.** Spring-induced scarring is not reflected as an anomaly on the vegetative health index at 30-meter spatial resolution.

Another consideration with our methodology is the relationship between study area size, volume of field data, and volume of background (pseudo-absence) points. Best practice considers around a 10:1 ratio of background points to field data points, a ratio we adhered to, generating 10,000 for the Mojave and Black Rock sites and 1,000 for our San Juans site. However, a potential source of uncertainty in pseudo-absence points is that they are not true confirmed absences but rather areas assumed to lack springs. This means some of these points could be near previously unknown springs, leading to misclassification. If this happens, it could confuse the model and reduce accuracy. The team also considered incorporating additional environmental variables, such as lineament density, bedrock geology, and distance from rivers, to strengthen our suitability detection models. Higher resolution of evapotranspiration and soil type data could have enhanced model detection accuracy and should be used in similar studies.

4. Conclusions

4.1 Interpretation of Results

This study demonstrated that it is feasible to use NASA Earth observations to link seasonal anomalies in land surface temperature and vegetative health, among other variables, with spring ecosystems in the American West. Of these variables, elevation, aspect (specifically northness), NDVI difference, land surface temperature, and drainage density were among the most useful in identifying candidate spring habitat areas and creating a predictive map of suitable locations where partners may find springs. Springs are a product of their hydrological environment, and thus it was not surprising to find that mid-higher elevations and cardinally oriented slopes were of the most suitable environments for spring ecosystems (Liu at al., 2024). Vegetative health and moisture indices were also useful for pinpointing areas retaining vegetation and high moisture conditions year-round, which are typically indicative of spring ecosystems (Qi et al., 2024). Spring ecosystems were often characterized by low drainage density, as expected, given the documented relationship between regions of low drainage density and re-emergence of groundwater discharge by springs (Arya et al., 2024; Carlston, 1963).

Habitat detection models offer a unique opportunity to explore a suite of environmental parameters that may be influencing the distribution of spring ecosystems. Habitat detection modeling through the Software for Assisted Habitat Modeling (SAHM) allowed for a powerful comparison of three models trained to predict suitable regions with spring ecosystems. When comparing the predictions of the three models across each study area, it was particularly interesting to note that all three models agreed on high suitability of spring occurrence along lineaments where, in reality, the underlying hydrological feature was a reservoir, river, or stream. While these features may be spring-fed, these instances likely resulted from low model specificity. Across all three models and study areas, MaxEnt had the highest sensitivity, and therefore, coupled with the highest AUC score, was the best predictor of suitable regions for spring ecosystems. Because of the low Cohen's Kappa values for these models, however, it is possible that the models are over-fitting to the training data and predictive results should be interpreted with caution. With higher-resolution satellite imagery of important predictor variables like NDVI, LST, and the incorporation of bedrock geology and soil type data, models may offer improved ability to identify spring-induced anomalies and cast predictions of regions suitable for spring ecosystems.

The team established correlations between spring ecosystems and environmental parameters like elevation, slope, aspect, drainage density, land surface temperature, and NDVI. These correlations may benefit project partners, who, based on these established relationships between spring ecosystems and environmental parameters and their familiarity with each respective region, may identify locations of interest for future field surveys or long-term monitoring of springs. These findings may also add to the scientific literature on spring ecosystems, providing new insight into the application of remote sensing to spring research, correlations between spring ecosystems and a suite of environmental variables, and finally, how these findings are specific to the understudied spring ecosystems of the American West.

4.2 Feasibility & Partner Implementation

The team discovered limitations of using NASA Earth observations to map springs, specifically acknowledging that the analyses were likely biased towards certain spring types and did not fully capture the complexities of all spring dynamics. Specifically, the use of land surface temperature, rather than an Earth observation measure of carbon dioxide emissivity, for example, favored the detection of geothermal springs over carbon dioxide springs. Additionally, spatiotemporal mismatches between satellite data and ground observations limited the team's ability to match up Earth observation anomalies with spring data collected by project partners during those years.

The project highlighted actionable strategies for project partners to integrate modeling approaches in longer-term monitoring efforts. For example, the MaxEnt models generated predictive maps of suitable spring locations throughout each partner's area of jurisdiction. These ensemble maps should enable the project partners to identify regions for future field surveys of spring ecosystems. In turn, improved field survey efforts may lead to longer-term, more comprehensive monitoring of spring ecosystems by project partners, allowing for research into the impacts of longer-term changes in climate to their ecosystems. Coupled with the remote sensing strategies outlined here, project partners will soon possess a powerful tool to identify regions for future field surveys and characterize long-term changes in spring ecosystems and the repercussions for conservation. Armed with this knowledge, project partners may make informed decisions on how to best manage spring ecosystems to protect the value of such special areas.

5. Acknowledgements

We would like to express our gratitude to the following individuals for their contributions to this project:

Partners:

- Sofia Andeskie (Mojave National Preserve, National Park Service)
- Jonah Blustain & Bradlee Matthews (Black Rock Desert, Bureau of Land Management, Winnemucca District Office)
- Dr. James Henriksen (The Two Frontiers Project)
- Connor Newman (United States Geological Survey, Colorado Water Science Center)

Center Lead:

- Truman Anarella (NASA DEVELOP at CO – Fort Collins)

Advisors:

- Dr. Tony Vorster (Colorado State University, Natural Resources Ecology Laboratory)
- Nicholas Young (Colorado State University, Natural Resources Ecology Laboratory)

NASA DEVELOP:

- Brooklyn Appling (Geoinformatics Fellow – Virginia LaRC)
- Aryssa Camenisch (CO – Fort Collins)
- Ambra Jacobson (CO – Fort Collins)
- Nancy Nthiga (CO – Fort Collins)
- Marisa Smedsrud (Geoinformatics Fellow – Virginia LaRC)
- Isabel Tate (Project Coordination Fellow – Alabama MSFC)

This material contains data from the Optical Land Imaging (OLI) and Thermal Infrared Sensors (TIRS) aboard Landsat 8 and 9 satellites (2024), processed by the U.S. Geological Survey (USGS).

This material contains data from the Standardized Precipitation-Evapotranspiration Index (SPEI) (2024), processed by Instituto Pirenaico de Ecología (Pyrenean Institute of Ecology) in Zaragoza, Spain.

This material also contains data from the National Elevation Dataset, processed by the U.S. Geological Survey (USGS).

Any opinions, findings, and conclusions or recommendations expressed in this material are those of the author(s) and do not necessarily reflect the views of the National Aeronautics and Space Administration.

This material is based upon work supported by NASA through contract 80LARC23FA024.

6. Glossary

2FP- Two Frontiers Project
3D Elevation Program (3DEP) - A USGS program that provides high-resolution elevation data products, including Digital Elevation Models (DEMs), to support applications such as aspect, slope, and drainage density.
ArcGIS Pro - A desktop Geographic Information System software used for mapping, spatial analysis, and geospatial data management and developed by Esri.
ArcMap- A component of Esri's ArcGIS suite of geospatial processing programs.
BLM – Bureau of Land Management
DEM - Digital Elevation Model
Drainage Density - A measure of the extent of the drainage network within a particular area.
Earth observations - Satellites and sensors that collect information about the Earth's physical, chemical, and biological systems over space and time.

Eastness – A measure of the directional component of slope towards the east.
Elevation - The height of a point above a reference level, typically the Earth's sea level.
Flow Accumulation Tool - A tool in GIS used to measure the accumulation of flow into a particular cell or area, helping to identify the path of water flow and the presence of water bodies like streams and rivers.
Flow Direction Tool- A tool used in GIS to calculate the direction in which water flows from each cell in a digital elevation model.
EPA- Environmental Protection Agency
GIS- Geographic Information Systems
GLM- Generalized Linear Model
Geospatial Data - Information linked to geographic locations and can be visualized, analyzed, and interpreted through remote sensing.
Kernel Density- A GIS non-parametric statistical tool used to estimate the probability density function of a random variable
Landsat 8 & 9 - Satellites operated by NASA and the USGS that provide high-resolution Earth imagery and remote sensing data.
Line Density Tool - A GIS tool used to create a raster that shows the concentration of linear features per unit area.
LST- Land Surface Temperature
Machine Learning Models - Algorithms that use data to learn patterns and make predictions.
MaxEnt- Maximum Entropy
NASA - National Aeronautics and Space Administration
NED- National Elevation Dataset
NDMI - Normalized Difference Moisture Index
NDVI - Normalized Difference Vegetation Index
NOAA- National Ocean and Atmospheric Administration
Northness - A measure of the directional component of slope towards the north.
NPS - National Park Service
OLI- Operational Land Imager
R- A programming language and software environment used for statistical computing and data analysis.
Raster Calculator - A tool used to apply mathematical functions or logical expressions to raster data, helpful for extracting streams based on flow accumulation values.
Raster to Polyline Tool - A GIS tool used to convert raster data into vector format, creating lines that represent the stream network.
RF- Random Forest
R.slope.aspect Tool- A GIS tool used to calculate the slope and aspect for each cell in a raster dataset.
SAHM – Software for predictive habitat suitability modeling, developed by USGS, that integrates statistical tools for distribution modeling.
SRTM - Shuttle Radar Topography Mission
Surface Reflectance - The fraction of sunlight that is reflected off the Earth's surface as observed by remote sensing satellites.
TIRS - Thermal Infrared Sensor
USFS- United States Forest Service
USGS - United States Geological Survey
USFWS- United States Fish and Wildlife Service
VisTrails- An open-source modeling software.
Wet Hand Test - A field method used to measure the depth of spring water.

7. References

Arya, V., & Rao, M. S. (2024). Groundwater Recharge Potential Index and artificial groundwater recharge in the alluvial soils of the middle Ganga Basin. Discover Applied Sciences, 6(7), 367. https://doi.org/10.1007/s42452-024-05851-z

Bureau of Land Management Collaborators (n.d.). Black Rock Desert-High Rock Canyon Emigrant Trails National Conservation Area. Bureau of Land Management. https://www.blm.gov/visit/black-rock-desert-high-rock-canyon-emigrant-trails-national-conservation-area

Carlston, C. W. (1963). Drainage density and streamflow. US Government Printing Office.

Casper, M. C., & Vohland, M. (2008). Validation of a large-scale hydrological model with data fields retrieved from reflective and thermal optical remote sensing data–A case study for the Upper Rhine Valley. Physics and Chemistry of the Earth, Parts A/B/C, 33(17-18), 1061-1067. https://doi.org/10.1016/j.pce.2008.06.001

Castellazzi, P., Gao, S., Pritchard, J., Ponce-Reyes, R., Stratford, D., & Crosbie, R. (2024). Detecting springs and groundwater-dependent vegetation in data-scarce regions of Australia combining citizen science, GRACE, and optical/radar imagery. Remote Sensing of Environment, 313, 114345. https://doi.org/10.1016/j.rse.2024.114345

Colorado Water Science. (2022). Data supporting management of thermal springs –Steamboat Springs, Colorado. U.S. Geological Survey. https://www.usgs.gov/centers/colorado-water-science-center/science/data-supporting-management-thermal-springs-steamboat

Dhakal, S., Subedi, R., Kandel, S., & Shrestha, S. (2024). Remote sensing and geospatial approach: Optimizing groundwater exploration in semi-arid region, Nepal. Heliyon, 10(10). https://doi.org/10.1016/j.heliyon.2024.e31281

Earthstar Geographics, Oregon State Parks, Esri, TomTom, Garmin, FAO, NOAA, USGS, EPA, & USFWS. (2024). Basemap data in ArcGIS Pro. Retrieved from ArcGIS Online.

Esri. (2024). ArcGIS Pro (Version 2.3.0.) [Software]. Environmental Systems Research Institute, Inc. https://www.esri.com/en-us/arcgis/

Esri. (2024). ArcGIS Pro (Version 2.3.1.) [Software]. Environmental Systems Research Institute, Inc. https://www.esri.com/en-us/arcgis/

Esri. (2024). Fill (Spatial Analyst). Environmental Systems Research Institute. https://pro.arcgis.com/en/pro-app/latest/tool-reference/spatial-analyst/fill.htm

Esri. (2024). Flow Accumulation (Spatial Analyst). Environmental Systems Research Institute. https://pro.arcgis.com/en/pro-app/latest/tool-reference/spatial-analyst/flow-accumulation.htm

Esri. (2024). Flow Direction (Spatial Analyst). Environmental Systems Research Institute. https://pro.arcgis.com/en/pro-app/latest/tool-reference/spatial-analyst/flow-direction.htm

Esri. (2024). Line Density (Spatial Analyst). Environmental Systems Research Institute. https://pro.arcgis.com/en/pro-app/latest/tool-reference/spatial-analyst/line-density.htm

Esri. (2024). Raster Calculator (Spatial Analyst). Environmental Systems Research Institute. https://pro.arcgis.com/en/pro-app/latest/tool-reference/spatial-analyst/raster-calculator.htm

Esri. (2024). Raster to Polyline (Conversion). Environmental Systems Research Institute. https://pro.arcgis.com/en/pro-app/latest/tool-reference/conversion/raster-to-polyline.htm

Esri. (2024). *World Imagery* [Basemap layer]. ArcGIS Pro.

Granata, F., Saroli, M., de Marinis, G., & Gargano, R. (2018). Machine learning models for spring discharge forecasting. Geofluids, 2018(1), 8328167. https://doi.org/10.1155/2018/8328167

Idi, B. Y., Maiha, A. I., & Abdullahi, M. (2022). Spatial mapping and monitoring thermal anomaly and radiative heat flux using Landsat-8 thermal infrared data–A case study of Lamurde hot spring, upper part of Benue trough, Nigeria. Journal of Applied Geophysics, 203, 104654. https://doi.org/10.1016/j.jappgeo.2022.104654

Liu, F., Conklin, M. H., & Shaw, G. D. (2024). Elevational control of isotopic composition and application in understanding hydrologic processes in the mid Merced River catchment, Sierra Nevada, California, USA. *Hydrology and Earth System Sciences*, *28*(10), 2239-2258. https://doi.org/10.5194/hess-28-2239-2024

Lipman, P. W., Steven, T. A., Luedke, R. G., & Burbank, W. S. (1973). Revised volcanic history of the San Juan, Uncompahgre, Silverton, and Lake City calderas in the western San Juan Mountains, Colorado. J. Res. US Geol. Survey, 1(6), 627-642.

Morissette, J. T., Richardson, A. D., Knick, S. T., & Busey, R. C. (2013). VisTrails SAHM: Visualization and workflow management for species habitat modeling. Ecography, 36(2), 129–135. https://doi.org/10.1111/j.1600-0587.2012.07815.x

Niraula, R. R., Sharma, S., Pokharel, B. K., & Paudel, U. (2021). Spatial prediction of spring locations in data poor region of Central Himalayas. *Hydrology Research*, *52*(2), 492-505. https://doi.org/10.2166/nh.2020.223

National Park Service Collaborators (n.d.-a) Mojave National Preserve. U.S. National Park Service. https://www.nps.gov/moja/index.htm

National Park Service Collaborators (n.d.-b) Rocky Mountain National Park. U.S. National Park Service. https://www.nps.gov/romo/index.htm

Pearl, R. H., Zacharakis, T. G., & Ringrose, C. D. (1983). Geothermal-resource assessment of the Steamboat-Routt Hot Springs area, Colorado. Resources Series 22 (No. DOE/ET/28365-24). Colorado Dept. of Natural Resources, Denver (USA). https://doi.org/10.2172/6345641

QGIS Development Team. (2018). QGIS Geographic Information System (Version 3.4.0 "Bratislava"). [Software]. Open Source Geospatial Foundation. Retrieved from https://qgis.org.

Qi, G., She, D., Xia, J., Song, J., Jiao, W., Li, J., & Liu, Z. (2024). Soil moisture plays an increasingly important role in constraining vegetation productivity in China over the past two decades. *Agricultural and Forest Meteorology*, *356*, 110193. https://doi.org/10.1016/j.agrformet.2024.110193

Reath, K. A., & Ramsey, M. S. (2013). Exploration of geothermal systems using hyperspectral thermal infrared remote sensing. *Journal of Volcanology and Geothermal Research*, *265*, 27-38. https://doi.org/10.1016/j.jvolgeores.2013.08.003

San Juan Mountains Association. (n.d.). *Chicago Basin trip planning*. San Juan Mountains Association. Retrieved March 11, 2025, from https://sjma.org/chicago-basin-trip-planning

Stevens, Lawrence E. "The springs biome, with an emphasis on arid regions." (2020): 354-370. https://doi.org/10.1016/B978-0-12-409548-9.12451-0

Talbert, C., & Talbert, M. (2001). *Software for Assisted Habitat Modeling (SAHM) [Computer software]*. U.S. Geological Survey, Fort Collins Science Center. Retrieved from https://www.usgs.gov/centers/fort-collins-science-center

U.S. Forest Service. (n.d.). Nature & science: San Juan National Forest. U.S. Forest Service. Retrieved March 11, 2025, from https://www.fs.usda.gov/detailfull/sanjuan/learning/nature-science/?cid=fseprd647665

U.S. Forest Service. (n.d.). *San Juan National Forest*. U.S. Department of Agriculture. Retrieved March 13, 2025, from https://www.fs.usda.gov/sanjuan

U.S. Geological Survey. (2023-2024). *National Elevation Dataset (NED) Level 1 10m TIF [Data set*]. U.S.Geological Survey. Retrieved from https://apps.nationalmap.gov/downloader/.

U.S. Geological Survey. (2024). *Landsat 8-9 OLI/TIRS Collection 2 Level 2 Surface Reflectance 30m TIF [Data set]*. U.S. Geological Survey EarthExplorer. Retrieved from https://earthexplorer.usgs.gov

U.S. Geological Survey. (2024). Landsat Normalized Difference Moisture Index | U.S. Geological Survey https://www.usgs.gov/landsat-missions/normalized-difference-moisture-index

U.S. Geological Survey. (2024). Landsat Normalized Difference Vegetation Index | U.S. Geological Survey. Landsat Normalized Difference Vegetation Index | U.S. Geological Survey

U.S. Geological Survey. (2024). Landsat Surface Temperature | U.S. Geological Survey https://www.usgs.gov/landsat-missions/landsat-surface-temperature

U.S. Geological Survey. (n.d.). *Wet-dry cycle: Black Rock Playa in Nevada*. U.S. Geological Survey Earthshots. Retrieved March 11, 2025, from https://eros.usgs.gov/earthshots/wet-dry-cycle#:~:text=Black%20Rock%20Playa%20in%20Nevada,during%20winter%20and%20early%20s

U.S. Geological Survey. (2023-2024). U.S. Geological Survey 3D Elevation Program (3DEP) National Elevation Dataset (NED) Digital Elevation Model (DEM) Data. Available from: https://www.usgs.gov/3d-elevation-program. Accessed March 2025.

U.S. Geological Survey. (2024). Landsat 8-9 Level 2 Surface Reflectance Data. USGS Earth Explorer. https://earthexplorer.usgs.gov/

Weather Spark. (n.d.). Average weather in San Juan, Colorado, Mexico: Year-round. Weather Spark. Retrieved March 11, 2025, from https://weatherspark.com/y/7314/Average-Weather-in-San-Juan-Colorado-Mexico-Year-Round#:~:text=The%20month%20with%20the%20most%20rain%20in%20San%20Juan%20Colorado,average%20rainfall%20of%200.1%20inches

Zhuang, Y., Fu, R., Lisonbee, J., Sheffield, A. M., Parker, B. A., & Deheza, G. (2024). Anthropogenic warming has ushered in an era of temperature-dominated droughts in the western United States. Science Advances, 10(45), eadn9389. https://doi.org/10.1126/sciadv.adn9389

8. Appendices

Appendix A – Preliminary Analyses of Predictor Variables

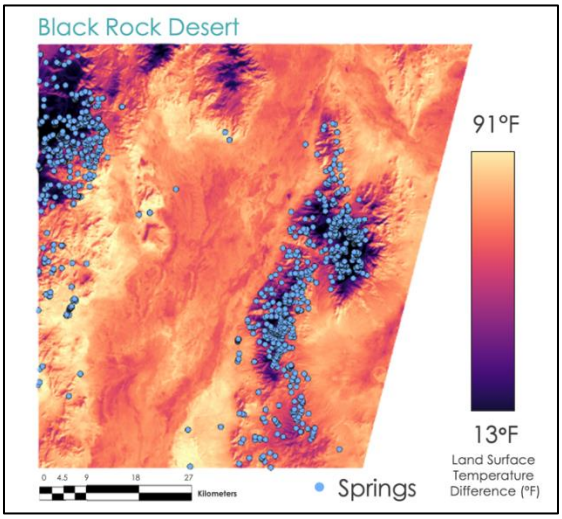

Figure A1. Land surface temperature (°F), as calculated from the Thermal Infrared Sensors aboard Landsat 8&9, across the Black Rock Desert of Nevada. Springs plotted in blue across the landscape.

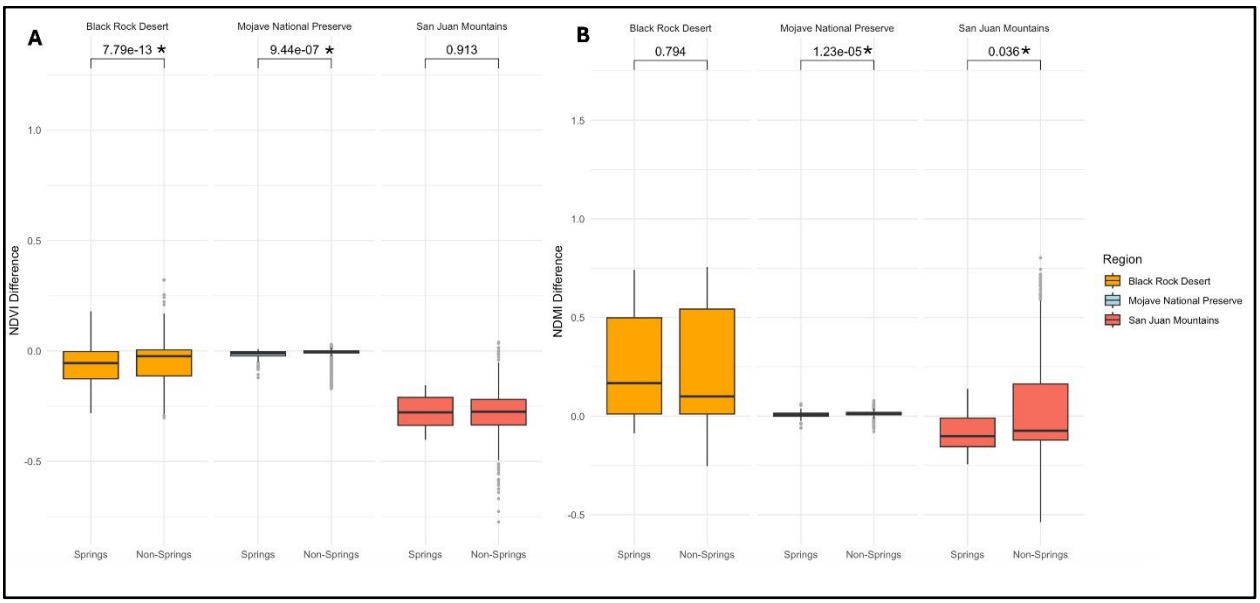

Figure A2. Seasonal differences in **A.** Normalized Differential Vegetation & **B.** Moisture Indices across each study site. Known spring point values compared with non-spring, pseudo-absence points with a T-test. Significant p values (<0.05) marked with a '*'.

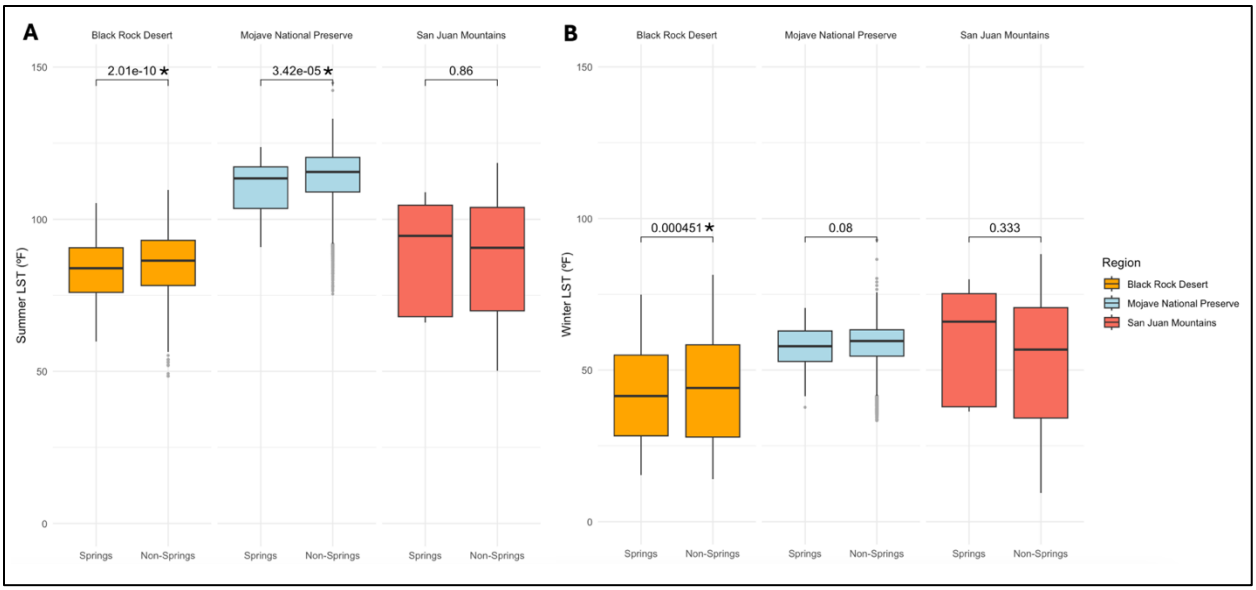

Figure A3. Seasonal (**A.** Summer, and **B.** Winter) land surface temperatures across each study site. Known spring point values compared with non-spring, pseudo-absence points with a T-test. Significant p values (<0.05) marked with a '*'.

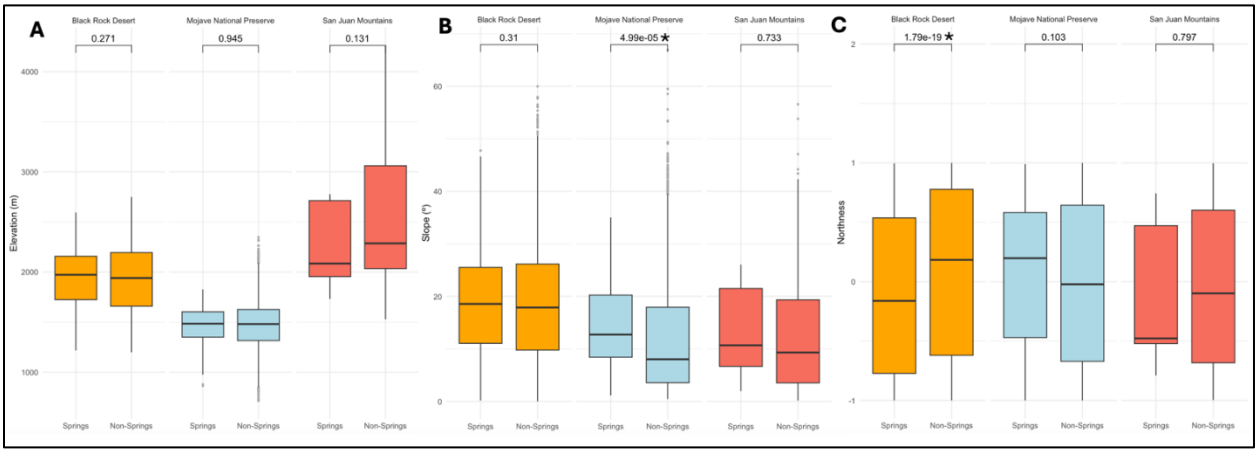

Figure A4. Topographical predictors of suitable spring locations. **A.** Elevation (m), **B.** Slope (º), and **C.** Aspect (Northness) characterizing spring and non-spring ecosystems. Known spring point values compared with non-spring, pseudo-absence points with a T-test. Significant p values (<0.05) marked with a '*'.

Appendix B – Results of Predictor Variable and Model Analysis

Figure B1. Confusion Matrix for Cross Validation Data

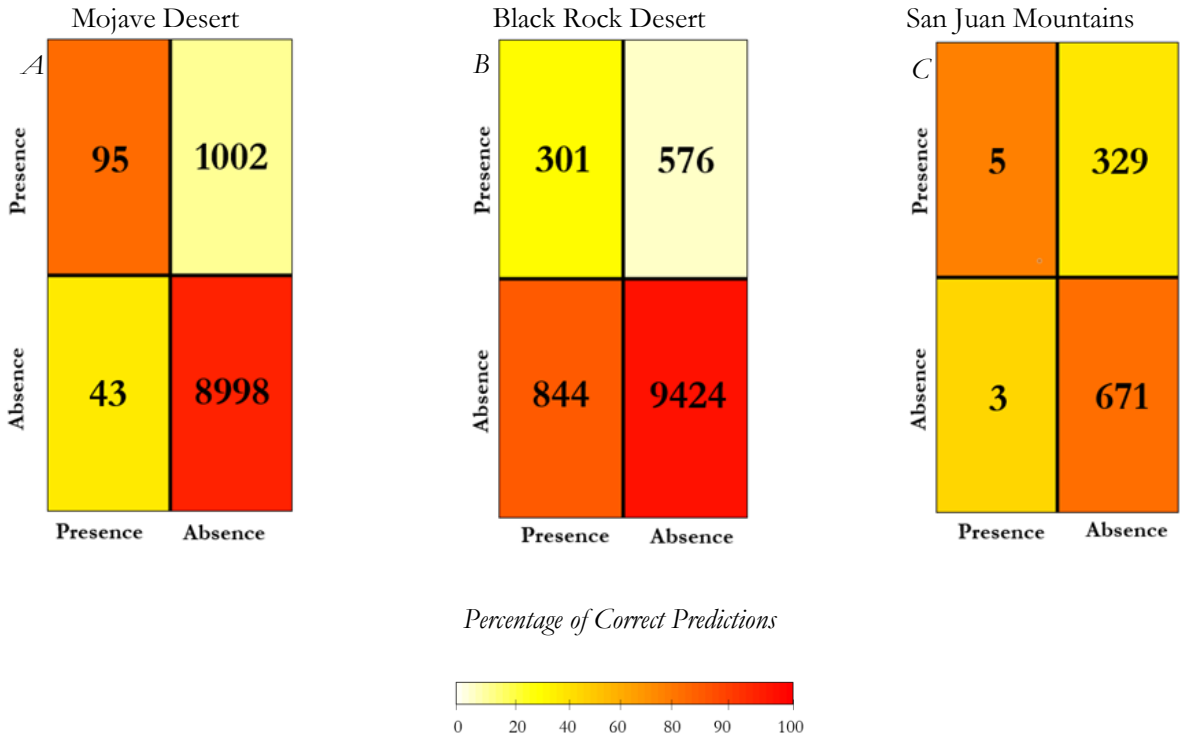

Figure B1. Comparative analysis of MaxEnt model performance across three study areas using confusion matrices derived from cross-validation. The color gradient reflects prediction accuracy of spring locations, showing variations in performance across the Mojave Desert (a), Black Rock Desert (b), and San Juan Mountains (c).

Figure B2. Importance via Change in AUC – Permuted Predictors

a) Mojave Desert

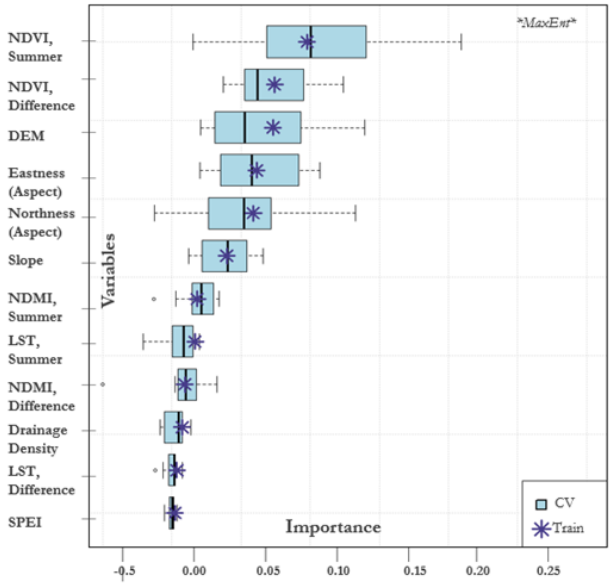

b) Black Rock Desert

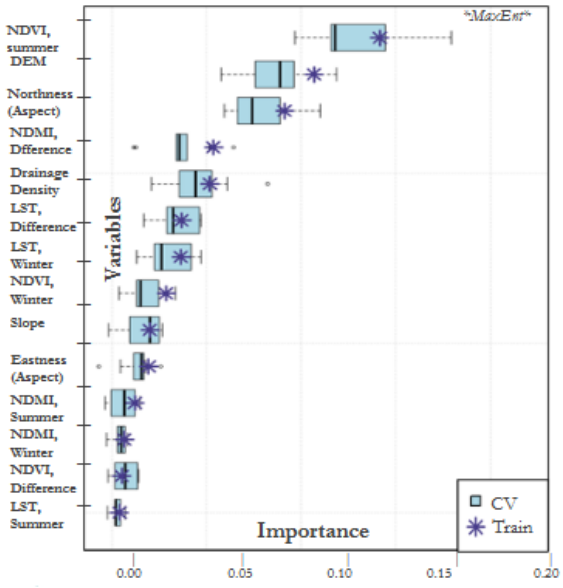

c) San Juan Mountains

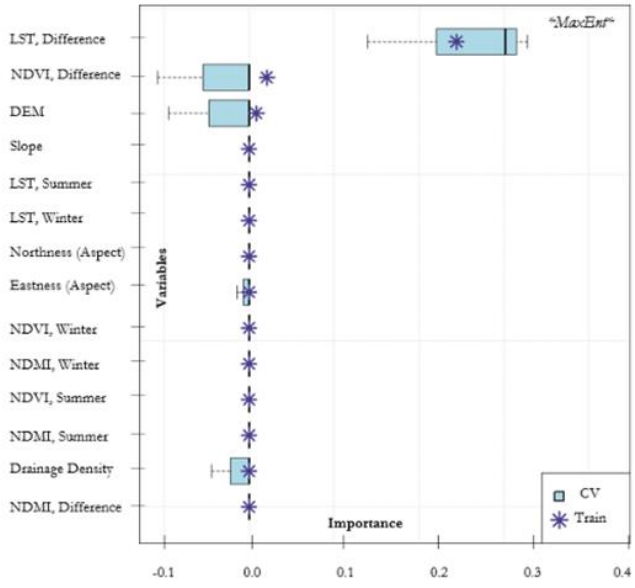

Figure B2. Predictor importance based on permuted change in AUC for spring presence models in the Mojave Desert (MaxEnt) (a), Black Rock Desert (MaxEnt) (b), and the San Juan Mountain Range (MaxEnt) (c). NDVI, DEM, LST, and topographic variables show the highest contributions.